Available online at www.sciencedirect.com
SCIENCE DIRECT®
ELSEVIER
Nuclear Physics A 723 (2003) 69–92
NUCLEAR PHYSICS A
www.elsevier.com/locate/npe

γ-ray angular distributions and correlations after projectile-fragmentation reactions

Andrew E. Stuchbery [1]

National Superconducting Cyclotron Laboratory, Michigan State University, East Lansing, MI, USA

Received 31 January 2003; accepted 14 March 2003

Abstract

The formulation required to interpret angular distribution and angular correlation measurements following projectile fragmentation reactions is outlined. Some concepts required to understand the observed fragment spin alignments and polarizations are discussed. Applications to in-beam spectroscopy using fragmentation reactions are considered, particularly in relation to γ-ray multipolarity measurements and spin assignments.

PACS: 23.20.En; 25.70.Mn; 24.70.+s; 25.60.-t

Keywords: γ-ray angular correlations/distributions; DCO; Spin assignments; Exotic nuclei; Polarization; Alignment; Intermediate-energy fragmentation and knockout reactions

1. Introduction

Over the past few decades in-beam γ-ray spectroscopy following heavy-ion-induced fusion–evaporation reactions has provided a great deal of information on nuclear structure. However, with stable beams and targets, studies are generally limited to neutron-deficient nuclei. Exotic nuclei far from stability can be studied by spectroscopic techniques following high- and intermediate-energy projectile fragmentation reactions. It is established that the fast-fragmentation process can lead to aligned and/or polarized (i.e., oriented) projectile fragments [1–9], so measurements of γ-ray angular distributions and γ–γ directional correlations from oriented (DCO) states can be made, at least in principle,

E-mail address: andrew.stuchbery@anu.edu.au (A.E. Stuchbery).

[1] Permanent address: Department of Nuclear Physics, Research School of Physical Sciences and Engineering, The Australian National University, Canberra, ACT 0200, Australia.

0375-9474/03/$ – see front matter
doi:10.1016/S0375-9474(03)01157-6

for the usual spectroscopic purpose of determining transition multipolarities and hence level spins. If a magnetic field or an electric field gradient is present at the nucleus it may also be possible to measure nuclear moments.

The present paper considers the application of angular distribution and angular correlation techniques to in-beam spectroscopy and the study of isomers populated by fragmentation reactions at beam energies of the order of 100A MeV. The purpose is to outline the formalism and principles with a view to (i) reaching a deeper understanding of reported polarizations [1,3] and alignments [2,4,6–9], and (ii) establishing possibilities for future experiments [10]. To this end, Section 2 briefly reviews some aspects of the fast fragmentation reaction mechanism and the resultant orientation of the fragment angular momentum. The general formalism for angular correlations is summarized in Section 3. Section 4 concerns the definitions of 'alignment' and 'polarization', and presents parametrizations of the m-substate population distribution for the evaluation of different types of alignment and polarization. A number of examples and applications of the angular correlation formalism are discussed in Section 5. This is followed by a summary and concluding remarks. Comparisons and contrasts with established applications to low-energy heavy-ion reactions will be drawn throughout the paper.

2. Reaction mechanism and angular momentum of projectile fragments

The fast projectile-fragmentation process results from a peripheral collision between projectile and target nuclei. A distinction must be drawn between direct reactions on loosely bound nuclei near the drip lines, in which one or two nucleons are knocked-out and discrete low-excitation states of the final nucleus are populated [11,12], and abrasion–evaporation reactions that lead to highly-excited fragments not so close to the drip lines. Reactions in this latter category are the main focus of the discussion in this section. The angular momentum of the fragments is determined primarily by a fast abrasion process in which nucleons are removed from the projectile (and target) nuclei leaving highly excited prefragments. These prefragments then de-excite by evaporating nucleons (and possibly clusters) until the remaining fragment is stable against further particle emission. The particle-evaporation cascade will reduce the angular momentum of the fragment and its orientation. After the particle evaporation is complete, the nucleus will typically be in a highly excited state and will decay, probably by a statistical γ-ray cascade, to the yrast states. In contrast with low-energy heavy-ion fusion–evaporation reactions, where the angular momentum may reach the stability limit, fragmentation reactions lead to high excitation energies with relatively low angular momentum [7,8,13].

The abrasion stage of the fragmentation reaction can result in fragments with aligned and/or polarized angular momenta. The general principle, first suggested by Asahi et al. [1–5], is that the target nucleus behaves as a spectator while conservation of momentum between the fragment and the abraded nucleons gives a preferred orientation for the fragment spin. (See Refs. [1–5] for further discussion.) In accord with this picture, it is found that both the polarization and the alignment are correlated with the linear momentum of the fragment. The qualitative trends in the experimental data can be explained in terms of this mechanism, but the magnitude of the polarization and the alignment is often

overestimated [3,14]. There are a number of simplifications in the implementations of the model reported to date [3] that could lead to this overestimation, one being that no account of the deorientation due to γ-ray emission is included. In preparation for an investigation of this matter, the present work includes aspects of the formalism required to model the loss of orientation in the statistical decay [15].

In the intermediate energy regime (20 to 200 MeV per nucleon) the fragmentation mechanism is accompanied by direct knockout and pick-up channels that contribute to the observed fragment yield, especially when the fragment mass is close to that of the projectile [16]. Since these processes all involve nucleon transfer to, and/or removal from, the nuclear surface, they are expected to give similar magnitudes for the spin alignment in the final fragment.

3. Angular correlation/distribution formalism

3.1. Notation and relation to previous work

In the following subsections the general formulae are summarized from which the angular distribution or directional correlation can be calculated for any of the situations of interest, particularly: (i) decays below isomers created in the fast-fragmentation process that survive transmission through a spectrometer [17,18], (ii) in-beam reactions at the production target [7–9], and (iii) in-beam spectroscopy following reactions of secondary fragments [11,12]. It is also sufficiently general to enable a correct treatment of the deorientation of the nuclear spin in the γ-ray cascade [14,15].

The formalism here is similar to that in Ref. [19], but there are some subtle differences and generalizations that make a restatement of the formalism necessary. It is assumed that the nuclei may be aligned or polarized by the reaction mechanism, but the polarization of the emitted γ-rays is not detected. The coordinate frame employed for evaluating the γ-ray distributions is always that in which the beam is directed along the positive z axis and the formalism used is essentially that of Alder and Winther [20]. However, the statistical tensors are not normalized (as they do) because this removes information that is required to calculate the correlations for all detector combinations in a multidetector array in such a way that they can be compared consistently on an equal footing, for example in a global fit to the whole data set. The normalization of the γ-ray distribution is therefore such that, in general, $\int W \, \mathrm{d}\Omega \neq 1$ (see below).

The present formulation is based on expressions given by Alder and Winther [20], which are also presented (with a few changes in notation) by Steffen and Alder in Ref. [21]. As far as possible the following discussion will use, or at least make connections with, the notations of Krane, Steffen and Wheeler [22], and Yamazaki [23], which are commonly used by those who work with γ-ray detector arrays.

Whereas the ‘beam axis’ is well defined in low-energy experiments, its meaning is not as obvious in fragmentation experiments where reaction products may be transported through a spectrometer to a target station where the γ-rays are observed. The term ‘beam axis’ is used here somewhat loosely, tacitly assuming that, where appropriate, any shift in the direction of the quantization axis is properly taken into account (see, e.g., Ref. [24]).

3.2. Angular correlation formalism

Fig. 1 shows the notation used to label the levels in a cascade of interest. The initial state of interest populated by the reaction (or by previously emitted unobserved γ ray cascades above the state of interest) is denoted I_1. Its orientation is specified by a statistical tensor [20] denoted $\rho_{k_1q_1}(I_1)$. The evaluation of the statistical tensor will be discussed in Section 3.3. This work assumes that the initial state can be aligned or polarized, but that no polarization of the γ radiation is detected. However, the formalism correctly tracks the polarization through a γ-ray cascade so that the ground-state statistical tensors applicable for β-decay measurements can be evaluated.

Consider now that the state I_1 decays to state I_2 by the emission of a γ-ray with multipolarities L and L'. If the γ ray is observed in a detector at the spherical polar angles θ_1 and ϕ_1 (in the coordinate frame where the z axis is the beam axis), the statistical tensor of the state I_2 becomes:

$$\rho_{k_2q_2}(I_2) = \sum_{k,q,k_1,q_1} \rho_{k_1q_1}(I_1)(-1)^{k_1+q_1}\sqrt{\frac{(2k+1)(2k_1+1)}{(2k_2+1)}}\begin{pmatrix} k_1 & k & k_2 \\ -q_1 & q & q_2 \end{pmatrix} \times A_k^{k_2k_1}(\delta_{\gamma_{12}}LL'I_2I_1)Q_k(E_{\gamma_{12}})D^{k*}_{q0}(\phi_1,\theta_1,0), \quad (1)$$

where $k_2 = 0, 1, 2, \ldots, 2I_2$ if I_2 is an integer, and $k_2 = 0, 1, 2, \ldots, 2I_2 - 1$ if I_2 is half-integer. (Similar relationships apply for k_1 and I_1.) If the state I_1 is not polarized or the polarization is not to be detected subsequently (e.g., if only γ-ray correlations or distributions with no detection of polarization are of interest), then k_1 and k_2 can be restricted to even values. $k = 0, 2, 4, \ldots, 2L_{\max}$, where $L_{\max}$ is the larger of L and L'. $q = -k, -k+1, -k+2, \ldots, 0, 1, 2, \ldots, k$. ($q_1$ and q_2 are likewise related to k_1 and k_2.)

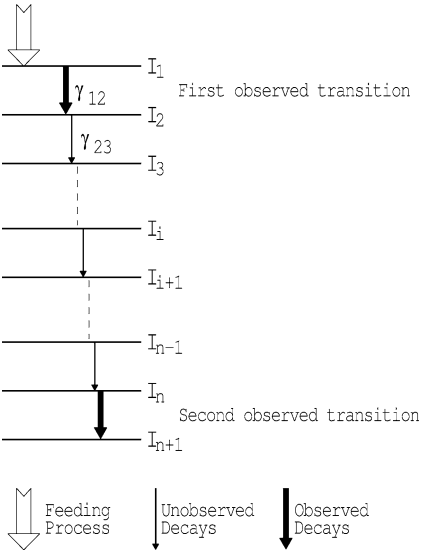

Fig. 1. Notation used to label levels in a general cascade.

The quantity $Q_k(E_{\gamma_{12}})$ is the solid-angle attenuation coefficient which takes account of the finite solid-angle opening of the γ-ray detector [25] and $D^k_{q0}(\phi,\theta,0)$ is the rotation matrix [20]. The expression in Eq. (1) applies in the case where the detector has axial symmetry about the direction of γ-ray emission. For γ rays emitted from rapidly moving nuclei the Lorentz transformation effectively distorts an otherwise axially symmetric detector. In this case the expression for emission of a photon into an element of solid angle at the spherical polar angles (θ_1,ϕ_1) is required. Within a normalization factor, this is obtained from Eq. (1) by replacing the Q_k coefficient by $\mathrm{d}\Omega_1 = \sin\theta_1 \mathrm{d}\phi_1$. (See Section 3.5.)

$A_k^{k_2k_1}(\delta_{\gamma_{12}} LL'I_2I_1)$ is related to the so-called generalized F-coefficient for the γ-ray transition between the states I_1 and I_2 with mixed multipolarities L and L' and mixing ratio $\delta_{\gamma_{12}}$ [20,22] by the expression:

$$A_k^{k_2k_1}(\delta LL'I_2I_1) = \frac{F_k^{k_2k_1}(LLI_2I_1) + 2\delta F_k^{k_2k_1}(LL'I_2I_1) + \delta^2 F_k^{k_2k_1}(L'L'I_2I_1)}{1+\delta^2}. \quad (2)$$

The F-coefficients are defined in Refs. [20,21] as

$$\begin{aligned} F_k^{k_2k_1}(LL'I_2I_1) \;=\; & (-1)^{L'+k_1+k_2+1}\sqrt{(2I_1+1)(2I_2+1)} \\ & \times \sqrt{(2L+1)(2L'+1)(2k+1)(2k_1+1)(2k_2+1)} \\ & \times \begin{pmatrix} L & L' & k \\ 1 & -1 & 0 \end{pmatrix} \begin{Bmatrix} I_2 & L & I_1 \\ I_2 & L' & I_1 \\ k_2 & k & k_1 \end{Bmatrix}. \end{aligned} \quad (3)$$

(Note that the expression for the generalized F coefficient given in Ref. [22] differs by a phase factor that is incorrect when odd-k_2 terms in the statistical tensor are required.)

The F-coefficients vanish unless a number of 'triangle' conditions are satisfied. In addition to the ranges of k, k_1 and k_2 noted above, there are also the conditions that

$$|L - L'| \leqslant k \leqslant L + L', \quad (4)$$

and

$$|k_1 - k_2| \leqslant k \leqslant k_1 + k_2. \quad (5)$$

If the γ ray is not observed, the statistical tensor $\rho_{k_2q_2}(I_2)$ may be evaluated by taking $k = 0$ only in Eq. (1); it then reduces to the form

$$\rho_{k_2q_2}(I_2) = U_{k_1}(\delta_{\gamma_{12}} LL'I_2I_1)\delta_{k_1k_2}\delta_{q_1q_2}\rho_{k_1q_1}(I_1), \quad (6)$$

where $\delta_{mm'}$ is the Kronecker delta symbol and the U-coefficients are [21]

$$U_k(\delta LL'I_2I_1) = \frac{U_k(I_1LI_2) + \delta^2 U_k(I_1L'I_2)}{1+\delta^2}, \quad (7)$$

where

$$\begin{aligned} U_k(I_1LI_2) \;&=\; \frac{F_0^{kk}(LLI_2I_1)}{\sqrt{(2k+1)}} \\ &=\; (-1)^{I_1+I_2+L+k}\sqrt{(2I_1+1)(2I_2+1)} \begin{Bmatrix} I_1 & I_1 & k \\ I_2 & I_2 & L \end{Bmatrix}. \end{aligned} \quad (8)$$

This expression is valid for odd-k as well as even-k, and does not change when I_1 and I_2 are interchanged.

Eq. (1) may be applied iteratively to propagate the statistical tensor along a cascade of any length, whether any individual transition is observed or not, until the final state of interest is reached. For the present purposes of investigating the behavior of γ-ray angular correlations and distributions after fragmentation reactions, a two-fold coincidence in the three-level sequence $I_1 \to I_2 \to I_3$ with no unobserved intermediate transitions will be sufficient.

The intensity of the γ-ray transition $I_2 \to I_3$ observed in a detector at polar angles (θ_2, ϕ_2), is determined from the statistical tensor of the state I_2 using the expression

$$W = \sum_{k_2,q_2} \rho_{k_2q_2}(I_2)\sqrt{(2k_2+1)}\,A_{k_2}(\delta_{\gamma_{23}}LL'I_3I_2)\,Q_{k_2}(E_{\gamma_{23}})D^{k_2*}_{q_20}(\phi_2,\theta_2,0), \tag{9}$$

where $A_{k_2}(\delta_{\gamma_{23}}LL'I_3I_2)$ is related to the 'ordinary' F-coefficients [22,23] by an expression of the same form as Eq. (2). The 'ordinary' F-coefficients are a special case of the generalized F-coefficient,

$$F_k(LL'I_2I_1) = F^{0k}_k(LL'I_2I_1) = (-1)^{L+L'}F^{k0}_k(LL'I_1I_2). \tag{10}$$

The remaining quantities in Eq. (9) are as defined for Eq. (1). Again, if the emission into an element of solid angle at (θ_2, ϕ_2) is required, Q_{k_2} should be replaced by $\mathrm{d}\Omega_2 = \sin\theta_2\,\mathrm{d}\phi_2$.

3.3. Statistical tensors

A statistical tensor, denoted $\rho_{kq}(I)$, specifies the orientation of the initial state. As the name implies, the statistical tensor applies to an ensemble of nuclei in a specified state, and is related to the distribution of magnetic substates with respect to a chosen coordinate frame. It is usually possible to specify the magnetic substate distribution by the populations $P(m)$ of the $2I+1$ m-substates. In this report it is assumed that the $P(m)$ are normalized so that $\sum_m P(m) = 1$.

For an m-substate distribution with axial symmetry, only the $q = 0$ components of $\rho_{kq}(I)$ are non-zero, and $\rho_{k0}(I)$ may be related to the statistical tensor often denoted $B_k(I)$ [23,26] by

$$\rho_{k0}(I) = \frac{B_k(I)}{\sqrt{2k+1}}, \tag{11}$$

where

$$B_k(I) = \sqrt{2I+1}\sum_m (-)^{I+m}\langle I - mIm|k0\rangle P(m). \tag{12}$$

$k = 0, 1, 2, \ldots, 2I$ if I is an integer, and $k = 0, 1, 2, \ldots, 2I-1$ if I is half-integer. For an *aligned* state $P(m) = P(-m)$ and only statistical tensors with even values of k are non-zero. For *polarized* states $P(m) \neq P(-m)$ and tensors with both even and odd values of k are non-zero.

Since the γ-ray angular correlation formalism uses a reference frame in which the beam axis is the z-axis, it may be necessary to transform the statistical tensor calculated in

a convenient 'reaction' frame (which might have axial symmetry) to the 'beam' frame, which is applicable for evaluation of the angular correlation. This is achieved by rotating the statistical tensor calculated in the 'reaction' frame into the 'beam' frame:

$$\rho_{kq}^{\text{beam}}(I) = \sum_{Q} \rho_{kQ}^{\text{reaction}}(I) D_{qQ}^{k}(\alpha, \beta, \gamma), \tag{13}$$

where (α, β, γ) is the Euler rotation that *rotates the beam frame into the reaction frame*.

In general, the orientation of a particular state may result from several reaction and decay processes, which could lead to different degrees of alignment and/or polarization. Despite this complication, the overall statistical tensor required is simply the weighted sum of those that contribute via the different population processes, i.e.,

$$\rho_{kq}(I) = \frac{\sum_i \eta_i \rho_{kq}^{i}(I)}{\sum_i \eta_i}, \tag{14}$$

where η_i is the relative fraction of the population of state I due to the mechanism i which results in the statistical tensor $\rho_{kq}^{i}(I)$.

3.4. Evaluation of the γ-ray correlations and distributions

Now that the general expressions required for the evaluation of angular distributions, angular correlations, or DCOs in any case of interest have been presented, some specific cases will be evaluated in this section. The expressions given apply in the rest frame of the nucleus and include the finite solid-angle correction factors (Q_k) for detectors with axial symmetry about the direction of γ-ray emission.

3.4.1. DCO

If Eq. (11), Eq. (1) and Eq. (9) are combined for the case of the $I_1 \to I_2 \to I_3$ cascade, the result is an expression for the DCO that is equivalent to the expressions given in Eqs. (9)–(12) of the paper by Krane, Steffen and Wheeler [22]. The expression is

$$\begin{aligned} &W(\theta_1, \phi_1, \theta_2, \phi_2) \\ &\quad = \sum_{k,q,k_1,q_1,k_2,q_2} \rho_{k_1 q_1}(I_1)(-1)^{k_1+q_1}\sqrt{(2k+1)(2k_1+1)} \begin{pmatrix} k_1 & k & k_2 \\ -q_1 & q & q_2 \end{pmatrix} \\ &\qquad\qquad \times A_k^{k_2 k_1}(\delta_{\gamma_{12}} L L' I_2 I_1) Q_k(E_{\gamma_{12}}) D_{q0}^{k*}(\phi_1, \theta_1, 0) \\ &\qquad\qquad \times A_{k_2}(\delta_{\gamma_{23}} L L' I_3 I_2) Q_{k_2}(E_{\gamma_{23}}) D_{q_2 0}^{k_2 *}(\phi_2, \theta_2, 0). \end{aligned} \tag{15}$$

Only in special cases can this expression be simplified. If required, the D-matrices can be related to spherical harmonics using $D_{q0}^{k*}(\phi, \theta, 0) = (-1)^q \sqrt{4\pi/(2k+1)}\, Y_{k-q}(\theta, \phi)$.

3.4.2. Angular correlation

If there is no orientation of the initial state, $\rho_{k_1 q_1}(I_1) = \delta_{k_1 0}\delta_{q_1 0}$. Inserting this into Eq. (15), the expression for the $I_1 \to I_2 \to I_3$ DCO, gives the general expression for the $I_1 \to I_2 \to I_3$ γ–γ correlation:

$$W(\theta_1,\phi_1,\theta_2,\phi_2) = \sum_k A_k^{k0}(\delta_{\gamma_{12}}LL'I_2I_1)A_k(\delta_{\gamma_{23}}LL'I_3I_2)Q_k(E_{\gamma_{12}})Q_k(E_{\gamma_{23}}) \times \sum_q D^{k*}_{q0}(\phi_1,\theta_1,0)D^{k*}_{q0}(\phi_2,\theta_2,0), \tag{16}$$

or, alternatively,

$$W(\theta_1,\phi_1,\theta_2,\phi_2) = \sum_k A_k^{k0}(\delta_{\gamma_{12}}LL'I_2I_1)A_k(\delta_{\gamma_{23}}LL'I_3I_2)Q_k(E_{\gamma_{12}})Q_k(E_{\gamma_{23}}) \times P_k(\cos\Theta), \tag{17}$$

where Θ is the angle between the two angles of γ-ray emission. Care must be taken not to confuse the sign of the mixing ratio and the order of the spin values if $A_k^{k0}(\delta_{\gamma_{12}}LL'I_2I_1)$ is evaluated in terms of the ordinary F_k coefficients:

$$A_k^{k0}(\delta LL'I_2I_1) = \frac{F_k(LLI_1I_2) + 2(-1)^{L+L'}\delta F_k(LL'I_1I_2) + \delta^2 F_k(L'L'I_1I_2)}{1+\delta^2}. \tag{18}$$

3.4.3. Angular distribution

Angular distributions may be evaluated directly from Eq. (9) by using the appropriate statistical tensor for the initial state. Replacing I_2 by I_i and I_3 by I_f for the initial and final states, respectively, gives

$$W(\theta,\phi) = \sum_{k,q}\rho_{kq}(I_i)\sqrt{(2k+1)}\,A_k(\delta_\gamma LL'I_fI_i)Q_k(E_\gamma)D^{k*}_{q0}(\phi,\theta,0), \tag{19}$$

which is applicable for a general orientation of the initial state. If this state has axial symmetry about the quantization axis only $q=0$ terms survive. Since $D^{k*}_{00}(\phi,\theta,0) = P_k(\cos\theta)$, Eq. (19) reduces to the more familiar expression

$$W(\theta) = \sum_k B_k(I_i)A_k(\delta_\gamma LL'I_fI_i)Q_k(E_\gamma)P_k(\cos\theta), \tag{20}$$

which can also be written in terms of the m-substate populations $P(m)$ by substituting Eq. (12), giving

$$W(\theta) = \sqrt{2I+1}\sum_{k,m}(-)^{I+m}\langle I-mIm|k0\rangle P(m)A_k(\delta_\gamma LL'I_fI_i) \times Q_k(E_\gamma)P_k(\cos\theta). \tag{21}$$

3.5. Lorentz boost

The angle between the beam axis and the direction of emission of the photon is affected if the nucleus is in motion rather than at rest. The relativistic velocity addition formulae can be used to show that the angles of emission in the laboratory, $(\theta_{\rm lab},\phi_{\rm lab})$, are related to those in the rest frame of the nucleus, $(\theta_{\rm nuc},\phi_{\rm nuc})$, by the expressions [27]

$$\cos\theta_{\rm lab} = \frac{\cos\theta_{\rm nuc}+\beta}{1+\beta\cos\theta_{\rm nuc}}, \tag{22}$$

$$\phi_{\rm lab} = \phi_{\rm nuc}, \tag{23}$$

where $\beta = v/c$ is the velocity of the nucleus along $\theta_{\rm lab} = \theta_{\rm nuc} = 0$. It follows that an element of solid angle in the rest frame is related to an element of solid angle in the laboratory frame by

$$\mathrm{d}\Omega_{\rm lab} = \frac{1-\beta^2}{(1+\beta\cos\theta_{\rm nuc})^2}\,\mathrm{d}\Omega_{\rm nuc}. \tag{24}$$

To obtain the correlation in the laboratory frame, $W_{\rm lab}(\theta_{\rm lab})$, from that in the rest frame of the nucleus, $W_{\rm nuc}(\theta_{\rm nuc})$, requires both transformation of the laboratory angle to the equivalent angle in the rest frame of the nucleus using Eq. (24), and multiplication by the appropriate solid-angle ratio so that the γ-ray flux emitted into 4π of solid angle is conserved, i.e.,

$$\int_{4\pi} W_{\rm lab}(\theta_{\rm lab})\,\mathrm{d}\Omega_{\rm lab} = \int_{4\pi} W_{\rm nuc}(\theta_{\rm nuc})\,\mathrm{d}\Omega_{\rm nuc}. \tag{25}$$

This condition is satisfied if

$$W_{\rm lab}(\theta_{\rm lab}) = W_{\rm nuc}(\theta_{\rm nuc})\frac{\mathrm{d}\Omega_{\rm nuc}}{\mathrm{d}\Omega_{\rm lab}}. \tag{26}$$

It is worth noting that the photon intensity observed in the laboratory frame is more strongly affected by the solid-angle factor than by the difference between $\theta_{\rm lab}$ and $\theta_{\rm nuc}$. The expression for an angular correlation (or DCO) is obtained in a straight-forward way:

$$W_{\rm lab}(\theta_{\rm 1lab},\phi_1,\theta_{\rm 2lab},\phi_2) = W_{\rm nuc}(\theta_{\rm 1nuc},\phi_1,\theta_{\rm 2nuc},\phi_2)\frac{\mathrm{d}\Omega_{\rm 1nuc}}{\mathrm{d}\Omega_{\rm 1lab}}\frac{\mathrm{d}\Omega_{\rm 2nuc}}{\mathrm{d}\Omega_{\rm 2lab}}. \tag{27}$$

A detector with axial symmetry about the direction of γ-ray emission in the laboratory frame does not have that symmetry in the rest-frame of the nucleus due to the Lorentz transformation. Hence the usual evaluations of the Q_k coefficients no longer apply. (These rely on (i) the angular correlation in the laboratory frame being expressed as a sum over spherical tensors, e.g., spherical harmonics, with angle-independent coefficients, and (ii) the detectors having axial symmetry about the specified direction of γ-ray emission.) In general the effects of finite sized detectors can be evaluated by putting $Q_k = 1$ in the expressions given above and averaging over the acceptance of the detector. Thus, for example, the measured angular distribution is

$$\overline{W} = \frac{\int W_{\rm lab}(\theta_{\rm lab},\phi_{\rm lab})\varepsilon(\theta_{\rm lab},\phi_{\rm lab})\,\mathrm{d}\Omega_{\rm lab}}{\int \varepsilon(\theta_{\rm lab},\phi_{\rm lab})\,\mathrm{d}\Omega_{\rm lab}}, \tag{28}$$

where $\varepsilon(\theta_{\rm lab},\phi_{\rm lab})$ is the detection efficiency along the direction specified by $(\theta_{\rm lab},\phi_{\rm lab})$ and the integration is over the solid angle subtended by the detector. Likewise, the expression for the angular correlation (or DCO) has the form

$$\overline{W} = \frac{\iint W_{\rm lab}(\theta_1,\phi_1,\theta_2,\phi_2)\varepsilon_1(\theta_1,\phi_1)\varepsilon_2(\theta_2,\phi_2)\,\mathrm{d}\Omega_1\,\mathrm{d}\Omega_2}{\iint \varepsilon(\theta_1,\phi_1)\varepsilon(\theta_2,\phi_2)\,\mathrm{d}\Omega_1\,\mathrm{d}\Omega_2}, \tag{29}$$

where the angles are now all understood to apply to the laboratory frame.

4. Alignment and polarization

4.1. Definitions of alignment and polarization

It has become conventional to report 'alignment' and 'polarization' as the ratio of an appropriately chosen statistical tensor to the value it takes when the orientation is maximized. As there is some variation in the terminology used in the literature, these quantities and their definitions are discussed here.

Alignment is defined in terms of the B_2 or ρ_{20} statistical tensor because the effect of the $k = 2$ term on the observables is usually much larger than the effect of the $k = 4$ term (e.g., in angular distribution measurements). Inserting Eq. (12) into Eq. (11) and evaluating the Clebsh–Gordan coefficient for $k = 2$ gives

$$\rho_{20}(I) = \sum_m \frac{2[3m^2 - I(I+1)]P(m)}{[(2I+3)(2I+2)(2I)(2I-1)]^{1/2}}. \tag{30}$$

In low-energy fusion–evaporation reactions, the angular momentum of the compound nucleus is aligned mainly in the plane perpendicular to the beam axis. It is appropriate therefore to define 'full' alignment for states with integer spins, $I = 1, 2, 3, \ldots$, as 100% occupation of the $m = 0$ substate, so that

$$\rho_{20}^{\max}(I) = \frac{-2[I(I+1)]}{[(2I+3)(2I+2)(2I)(2I-1)]^{1/2}}. \tag{31}$$

The alignment, denoted A_{O}, is then defined as

$$A_{\mathrm{O}} = \frac{\rho_{20}(I)}{|\rho_{20}^{\max}(I)|} = \sum_m \frac{[3m^2 - I(I+1)]P(m)}{I(I+1)}. \tag{32}$$

For fully oblate-aligned half-integer spins, $I = 3/2, 5/2, 7/2, \ldots$, the population is equally distributed in the $m = \pm 1/2$ substates so, following the same convention as for oblate-aligned integer spins, it follows that

$$A_{\mathrm{O}} = \frac{\rho_{20}(I)}{|\rho_{20}^{\max}(I)|} = \sum_m \frac{[3m^2 - I(I+1)]P(m)}{I(I+1) - 3/4}. \tag{33}$$

The $k = 2$ statistical tensor is negative when the population of the $m = 0$ substate dominates and the alignment is referred to as 'oblate'. Oblate alignment can also occur in fast-fragmentation reactions, especially for fragments with a linear momentum in the wings of the Goldhaber distribution [2,4]. For fragments near the center of the distribution 'prolate' alignment is expected and has been observed [2,4,6]. Prolate alignment means that the angular momentum of the fragment tends to be aligned parallel and antiparallel to the beam axis. In such cases it may be more convenient to define 'full alignment' as the situation where only the magnetic substates with $m = \pm I$ are populated ($P(I) = P(-I) = 0.5$). It then follows that

$$\rho_{20}^{\max}(I) = \frac{2[3I^2 - I(I+1)]}{[(2I+3)(2I+2)(2I)(2I-1)]^{1/2}}, \tag{34}$$

and

$$A_{\rm P} = \frac{\rho_{20}(I)}{|\rho_{20}^{\rm max}(I)|} = \sum_m \frac{[3m^2 - I(I+1)]P(m)}{I(2I-1)}. \tag{35}$$

In the special case of $I = 2$, $A_{\rm O}$ and $A_{\rm P}$ are equal, but they are not the same in general. Care should be taken about which definition is being used. Note that $A_{\rm O}$ can exceed 100% for high-spin states that are actually prolate aligned. For example a fully prolate-aligned 8^+ state has $A_{\rm O} = 5/3$. As defined here, the sign of the alignment is always the same as the sign of the $k = 2$ statistical tensor.

Whereas alignment is defined in the frame where the beam is along the quantization axis (i.e., the beam axis is the z-axis), the polarization is usually defined in a frame where the quantization axis is perpendicular to the beam. This frame is referred to here as the 'reaction' frame.

The *polarization* in the *reaction frame* is defined as $\langle I_z/I\rangle = \rho_{10}(I)/\rho_{10}^{\rm max}(I)$. In terms of the population parameters $P(m)$, it is clear that

$$\langle I_z/I\rangle = \sum_m m P(m)/I. \tag{36}$$

The same expression for the polarization results from considering the ratio of the $k = 1$ statistical tensor to its value for maximum polarization, i.e., when $P(I) = 1$, and $P(m) = 0$ otherwise. Specifically,

$$\rho_{10}(I) = -\sum_m \frac{m P(m)}{\sqrt{I(I+1)}}, \tag{37}$$

$$\rho_{10}^{\rm max}(I) = \frac{-I}{\sqrt{I(I+1)}}, \tag{38}$$

hence, by definition, the polarization is

$$\frac{\rho_{10}(I)}{\rho_{10}^{\rm max}(I)} = \sum_m m P(m)/I = \langle I_z/I\rangle. \tag{39}$$

The definition of alignment used here is the usual definition in the literature related to β-NMR and projectile-fragmentation studies. In papers on polarization by the tilted-foil technique [28,29] the polarization has also been defined as $\langle I_z\rangle/\sqrt{I(I+1)} = |\rho_{10}(I)|$.

4.2. Parametrization of the orientation

A parametrization of the substate distribution $P(m)$ for the cases of oblate alignment, prolate alignment and polarization is required in order to develop an appreciation for the types of angular correlations and distributions that can result from fragmentation reactions. For the present purposes simple functional forms are chosen for convenience with no attempt to provide a physical justification.

For oblate alignment, $P(m)$ is often approximated by a Gaussian distribution [23] of the form

$$P(m) = \frac{\exp(-m^2/2\sigma^2)}{\sum_{m'=-I}^{I} \exp(-m'^2/2\sigma^2)}, \tag{40}$$

where σ/I is treated as a parameter.

Gaussian distributions can also be assumed for prolate alignment and polarization. In these cases the Gaussian is centered about $M = \pm I$ for prolate alignment and about $m = +I$ for polarization. Specifically, for prolate alignment

$$P(m) = \frac{\exp[-(I - |m|)^2/2\sigma^2]}{\sum_{m'=-I}^{I} \exp(-m'^2/2\sigma^2)}, \tag{41}$$

and for polarization

$$P(m) = \frac{\exp[-(I - m)^2/2\sigma^2]}{\sum_{m'=-I}^{I} \exp(-m'^2/2\sigma^2)}. \tag{42}$$

Table 1 shows how $P(m)$ varies with m for a spin $I = 2$ state when $\sigma/I = 0.3$ and 0.6 in the cases of oblate alignment, prolate alignment, and polarization. Table 2 lists the corresponding orientation parameters $B_k = \sqrt{2k+1}\rho_{k0}$ $(k = 1, 2, 3, 4)$.

Figs. 2–4 show the relationship between the parameter σ/I and the alignment or polarization as defined in Section 4.1. Note that the alignment (proportional to $B_2(I)$) and polarization (proportional to $B_1(I)$) do not depend on the functional form of $P(m)$. This

Table 1
Population distributions $P(m)$ for $I = 2$

m	$P(m)$					
	σ/I oblate alignment[1]		σ/I prolate alignment[2]		σ/I polarization[3]	
	0.3	0.6	0.3	0.6	0.3	0.6
+2	0.003	0.086	0.400	0.273	0.798	0.499
+1	0.166	0.243	0.100	0.193	0.199	0.353
0	0.664	0.343	0.002	0.068	0.003	0.124
−1	0.166	0.243	0.100	0.193	0.000	0.022
−2	0.003	0.086	0.400	0.273	0.000	0.002

[1] See Eq. (40).
[2] See Eq. (41).
[3] See Eq. (42).

Table 2
Statistical tensors $B_k(I)$ for a state of spin $I = 2$ evaluated from the population distributions in Table 1

k	B_k					
	σ/I oblate alignment		σ/I prolate alignment		σ/I polarization	
	0.3	0.6	0.3	0.6	0.3	0.6
1	0	0	0	0	−1.269	−0.937
2	−0.985	−0.496	0.834	0.341	0.831	0.226
3	0	0	0	0	−0.283	0.116
4	0.712	0.008	0.000	−0.157	0.005	−0.067

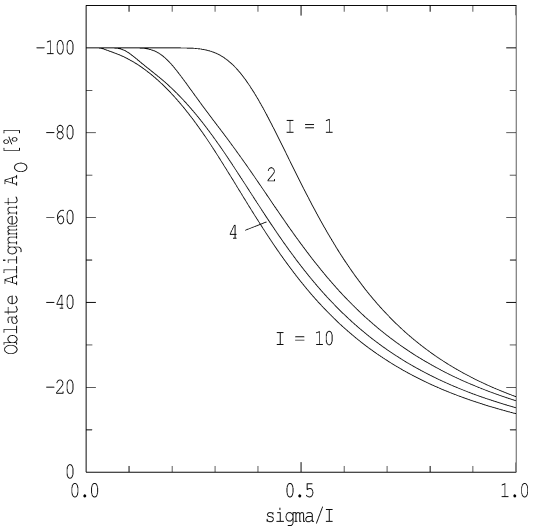

Fig. 2. Relationship between oblate alignment, Eq. (32), and the parameter σ/I when the m-substate distribution $P(m)$ is given by Eq. (40).

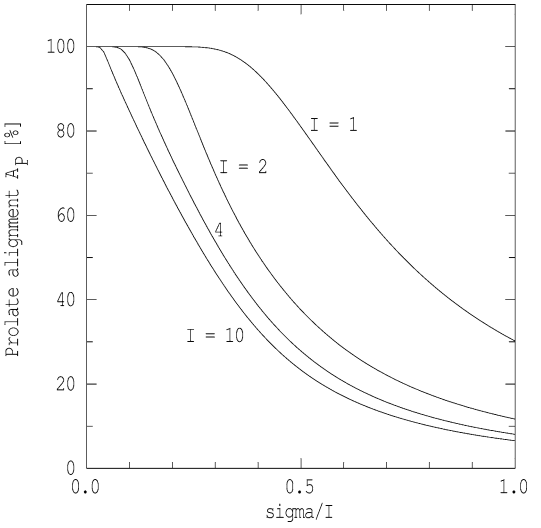

Fig. 3. Relationship between prolate alignment, Eq. (35), and the parameter σ/I when the m-substate distribution $P(m)$ is given by Eq. (41).

can be determined experimentally only by comparing the B_k values for different values of k. For given σ/I the alignment and the polarization become insensitive to I at high spin. It is not clear at present whether the Gaussian parametrizations used here are the most appropriate choice for fragmentation reactions. This, however, has little consequence for the present discussion.

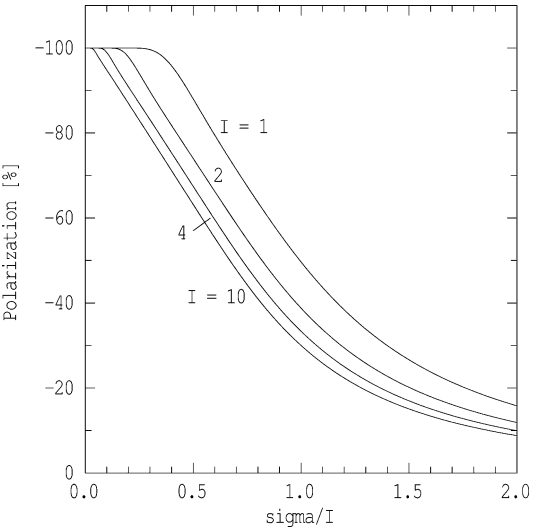

Fig. 4. Relationship between polarization $\langle I_z/I \rangle$, Eq. (39), and the parameter σ/I when the m-substate distribution $P(m)$ is given by Eq. (42).

5. Examples and applications

This section presents some examples and applications of the formalism to fragmentation reactions. The formalism could also be applied to Coulomb excitation [30,31] and inverse scattering, e.g., $(\mathrm{p}, \mathrm{p}')$ reactions [31], however, these cases are not specifically considered here. Section 5.1 begins pedagogically with examples of angular distributions from fully aligned prolate and oblate states and a fully polarized state. It then shows the angular distributions of partially aligned states in the rest frame of the nucleus, for different γ-ray transition multipolarities, and finally includes examples of the effect of the Lorentz boost. Section 5.2 considers the γ-ray angular distributions that result from direct knockout reactions. The γ–γ correlations depopulating aligned states (e.g., isomers) are considered in Section 5.3, and finally some aspects of perturbed angular correlations are discussed in Section 5.4.

Most of the examples presented below assume an alignment of $\sim 50\%$. This value is chosen because (i) it is large enough to give observable anisotropies, and (ii) the angular distribution ratios for quadrupole and dipole transitions reported by Azaiez et al. [7] and Sohler et al. [9] seem to require about 50% alignment. Measurements of ground-state alignments via β-delayed γ-ray emission or LMR techniques [2,6] generally report lower values. Time differential perturbed angular distribution (TDPAD) g factor measurements on isomeric states of projectile fragments that have been stopped in an applied magnetic field have been reported in Refs. [4,32]. In one case the alignment is about 35% in the center of the momentum distribution [4], but in the other [32] much lower net alignments ($\sim 2\%$) were observed (which may be mainly due to hyperfine interactions during flight through the spectrometer and only partly due to the reaction mechanism). Clearly, reaching a quantitative understanding of the alignment process in fragmentation reactions is an

important consideration for future γ-ray spectroscopy. This subject will be discussed in greater detail elsewhere [15].

5.1. γ-ray angular distributions from fast fragments

It is instructive to begin by considering the angular distributions in the rest frame of the nucleus so that the angular distributions for prolate alignment can be compared with those for oblate alignment, which is familiar from γ-ray spectroscopy with low-energy reactions.

Fig. 5 shows the γ-ray angular distributions from a fully prolate-aligned state, a fully oblate-aligned state and a fully polarized state. For the aligned states in this figure the quantization (and orientation) axis is the beam axis while for the polarized state the orientation axis is at 90 degrees to the beam (along the y-axis). The angular distributions are in the y–z plane. It is apparent that, as expected, the γ-ray angular distributions from the prolate-aligned and the polarized states are identical but for the 90° shift in the orientation axis.

A selection of transitions originating from oblate-aligned states with $\sigma/I = 0.5$, and hence $\approx 50\%$ alignment, is given in Fig. 6. The same transitions originating from prolate-aligned states, again with approximately 50% alignment ($\sigma/I = 0.4$), are presented in Fig. 7. No mixed-multipolarity transitions are included. The shapes of the angular distributions from prolate aligned states are *roughly* like those from the oblate shapes if 90° is subtracted from the detection angle. Note that the ambiguity between a stretched E2 transition and an $I \to I$ dipole is present for both prolate- and oblate-aligned states.

Figs. 8–11 show the same distributions in the laboratory frame where the nucleus is moving along the beam direction with $\beta = v/c = 0.3$. As expected, the ambiguities present in the $\beta = 0$ data remain for $\beta \neq 0$. The γ-ray intensity is strongly focused to forward

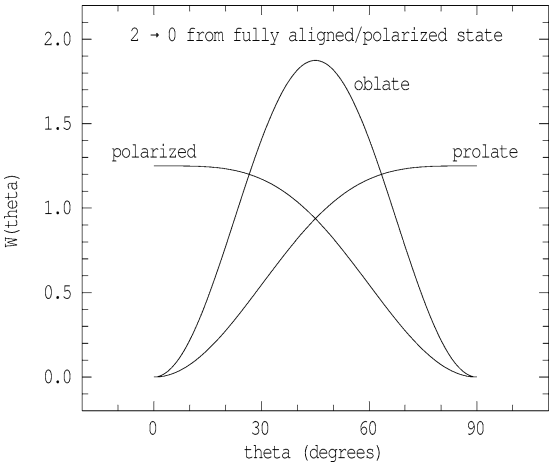

Fig. 5. Comparison of angular distributions, in the rest frame of the nucleus, for $2 \to 0$ transitions from a fully aligned or fully polarized initial state. The beam is along the z-axis, which is the quantization axis for the alignment. Theta is the angle between the quantization axis and the direction of γ-ray emission. The polarized state is oriented along the y axis. All distributions are in the y–z plane. Note that the distributions for prolate alignment and polarization are identical but for the 90° shift in the orientation axis.

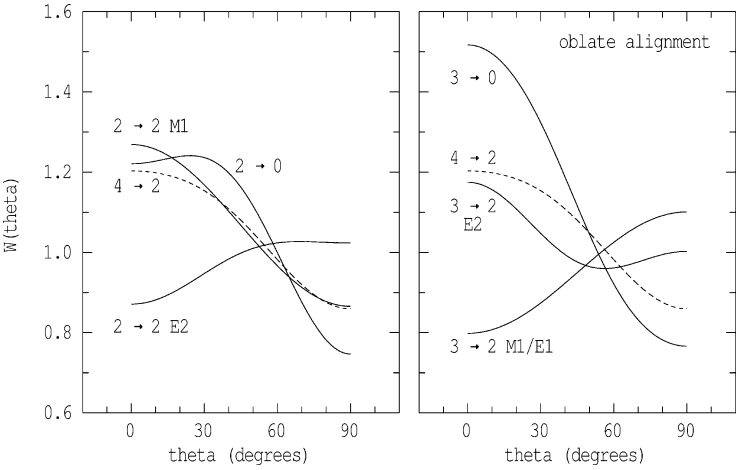

Fig. 6. Comparison of angular distributions, in the rest frame of the nucleus, for selected transitions from initial states with $\sim 50\%$ oblate alignment. The distribution for the $4 \rightarrow 2$ transition is included in both panels to provide a reference.

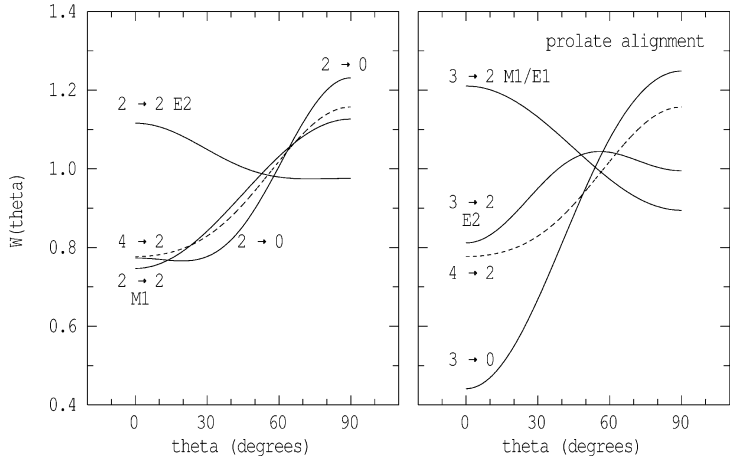

Fig. 7. Comparison of angular distributions, in the rest frame of the nucleus, for selected transitions from initial states with $\sim 50\%$ prolate alignment. The distribution for the $4 \rightarrow 2$ transition is included in both panels to provide a reference.

angles to the extent that all of the distributions in the lab frame are peaked at 0° and fall toward 180°.

The prominent effect of the Lorentz boost must be considered carefully if angular-distribution measurements are to be employed to determine γ-ray multipolarities and make spin assignments on rapidly moving fragments. It is clear from the figures (Figs. 8–11) that the γ-ray intensity at 0° to the beam is most sensitive to the spin change and multipolarity; however γ-ray measurements near 0° may compete with fragment detection requirements. The magnitude of the alignment and whether it is prolate or oblate in nature

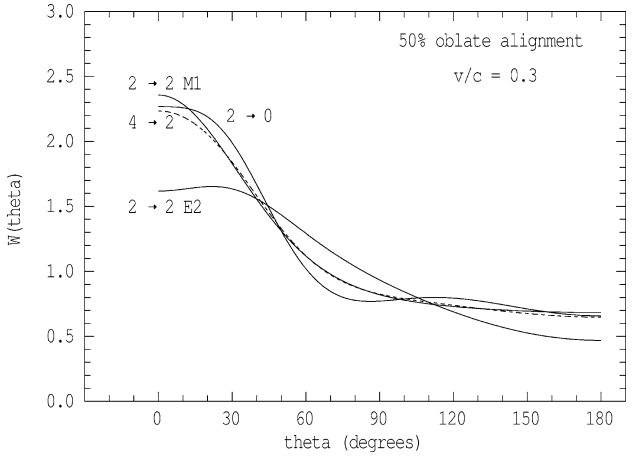

Fig. 8. Comparison of angular distributions from initial states with oblate alignment, as in the left-hand panel of Fig. 6, after a Lorentz boost of $\beta = v/c = 0.3$ along $\theta = 0°$.

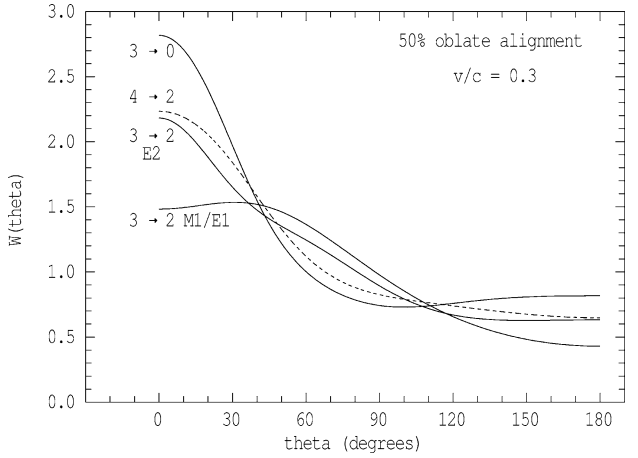

Fig. 9. Comparison of angular distributions from initial states with oblate alignment, as in the right-hand panel of Fig. 6, after a Lorentz boost of $\beta = v/c = 0.3$ along $\theta = 0°$.

can be determined by measuring the angular distribution of a known transition. Evidently detectors placed in the forward hemisphere are more sensitive to the intrinsic shape of the angular distribution than detectors in the backward hemisphere.

5.2. Angular distributions after direct reactions

Precision spectroscopy can be performed via single-nucleon and two-nucleon knockout reactions in inverse kinematics at typical energies of 50–1000 MeV/nucleon [11,12]. In these experiments the shapes of the parallel momentum distributions of the projectile residues determine the orbital angular momentum values, while the absolute cross sections

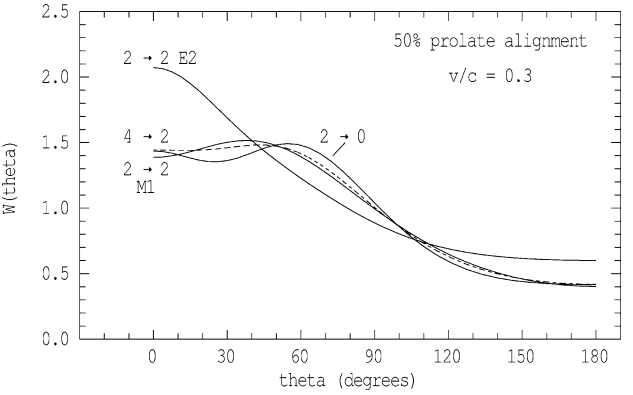

Fig. 10. Comparison of angular distributions from initial states with prolate alignment, as in the left-hand panel of Fig. 7, after a Lorentz boost of $\beta = v/c = 0.3$ along $\theta = 0°$.

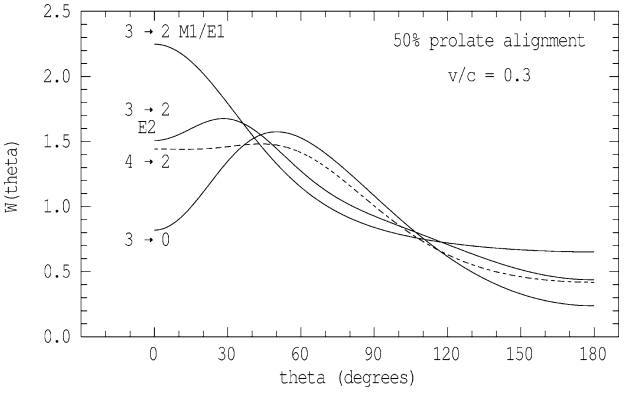

Fig. 11. Comparison of angular distributions from initial states with prolate alignment, as in the right-hand panel of Fig. 7, after a Lorentz boost of $\beta = v/c = 0.3$ along $\theta = 0°$.

to specific final levels give spectroscopic factors [11,12]. The cross sections to the magnetic substates populated in single-nucleon knockout reactions can be calculated, and from them the γ-ray angular distributions can be calculated. Analytical expressions valid for 'halo' states have been given for $l = 0, 1$ [33] and $l = 2$ [34]. The cross sections, σ_{knockout}, for normal bound states can be evaluated numerically in eikonal theory [11,12]. It is found quite generally for single-nucleon knockout that the $m = \pm l$ states are favored.

Fig. 12 shows examples of angular distributions for γ-rays depopulating a spin $5/2$ state in ^{27}Na populated by proton knockout on ^{28}Mg. These are evaluated taking $P(m) = \sigma_{\text{knockout}}(I, m)$, with the values $\sigma_{\text{knockout}}(5/2, 1/2) = 5.7$, $\sigma_{\text{knockout}}(5/2, 3/2) = 6.6$, $\sigma_{\text{knockout}}(5/2, 5/2) = 12.8$ [35]. The alignment is prolate with a magnitude of approximately 30% that is sufficient to give rise to observable effects. This may have implications for the correct evaluation of spectroscopic factors from the fragment-γ-ray coincidence data, or alternatively, provide an additional tool to assign level spins.

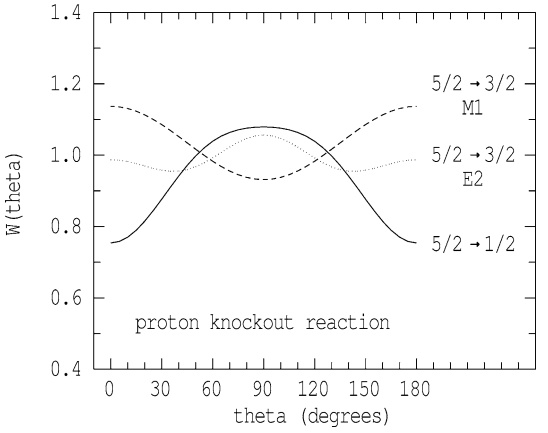

Fig. 12. Angular distributions in the rest frame of the nucleus for decays from the first-excited spin 5/2 state in ^{27}Na populated by a direct proton knockout reaction on ^{28}Mg. The alignment is about 30% prolate.

There is considerable scope for extending this work. For example, the formalism for evaluating two-proton knockout has not yet been derived rigorously, but there are suggestions that the alignment may become oblate in that case [35]. Also, it is possible to evaluate correlations between the direction of the emitted γ-ray and the center-of-mass direction of the fragment, which would be expected to exhibit a larger anisotropy than the corresponding angular distribution (in which the fragment direction is not considered).

Whilst discussing secondary reactions on fast fragments it should be noted that the spin orientation achieved for secondary fragments with spins $I \geqslant 1$ may be affected by the orientation produced in the primary reaction. However, in those cases where the secondary beam is an even–even nuclide, and hence has a spin zero ground state, no orientation produced in the primary reaction can be passed onto the secondary reaction process.

5.3. Angular correlations and DCOs

Since γ–γ correlations following the decays of unoriented nuclei at rest are well known they need no elaboration here. There may, however, be applications where γ–γ correlations below stopped isomeric states, which have been oriented by the reaction, may be of interest. Fig. 13 shows examples of γ–γ correlations below an aligned state with spin 8, which is assumed to have either a prolate or an oblate alignment of $\sim 50\%$. The correlations for two quadrupole transitions and a sequence of a quadrupole and a dipole transition (or vice versa) are shown. The shapes of these correlations are typical for the sequences of transition multipolarities, largely independent of the initial spin value. It is clear that the γ–γ correlation is strongly affected by alignment in the initial state and that the correlations for prolate- and oblate-aligned initial states differ considerably. The presence of an appreciable alignment, if not properly taken into account, could give incorrect transition intensities or false multipolarity assignments.

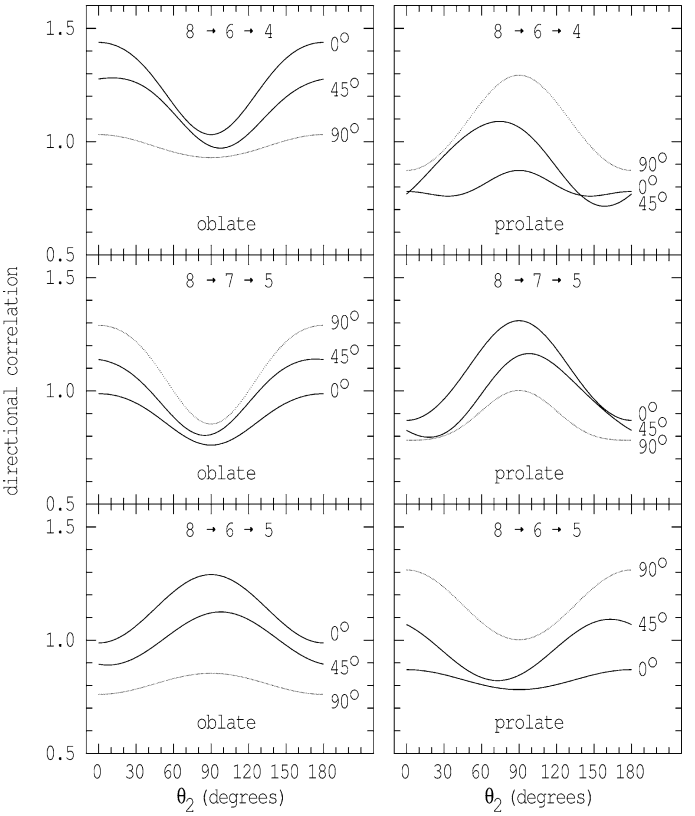

Fig. 13. γ–γ angular correlations (or DCOs) from aligned initial states with spin 8. The left panels have oblate alignment and the right panels have prolate alignment. The upper panels are for two quadrupole transitions in the spin sequence $8 \rightarrow 6 \rightarrow 4$, the middle panels are for a dipole and a quadrupole transition in the spin sequence $8 \rightarrow 7 \rightarrow 5$, and the lower panels are for a quadrupole and a dipole transition in the spin sequence $8 \rightarrow 6 \rightarrow 5$. θ_1 is the angle (with respect to the quantization axis) at which the first transition (either $8 \rightarrow 6$ or $8 \rightarrow 7$) is detected, while θ_2 is the angle at which the second transition ($6 \rightarrow 4$, $6 \rightarrow 5$ or $7 \rightarrow 5$) is detected. The θ_1 angles are indicated to the right of the curves.

5.4. Perturbed angular correlations and distributions

The evaluation of perturbed angular correlations/distributions is largely outside the scope of the present paper because, as a generalization, fast fragments are completely stripped of electrons and there can be no perturbation. However in cases where fragments are slowed to a velocity regime where the ions can carry electrons, and the ion emerges into vacuum, there will be a perturbation of the angular distribution that must be understood whether the intention is to measure the γ-ray multipolarity or deduce a nuclear moment. Some of the relevant formulae and an example will be given here.

The fields produced by atomic electrons bound to a free ion moving in vacuum have traditionally be divided into two classes—so-called ‘cold’ ionization where the ion carries very few electrons in the lowest available orbits, and so-called ‘hot’ ionization, in which

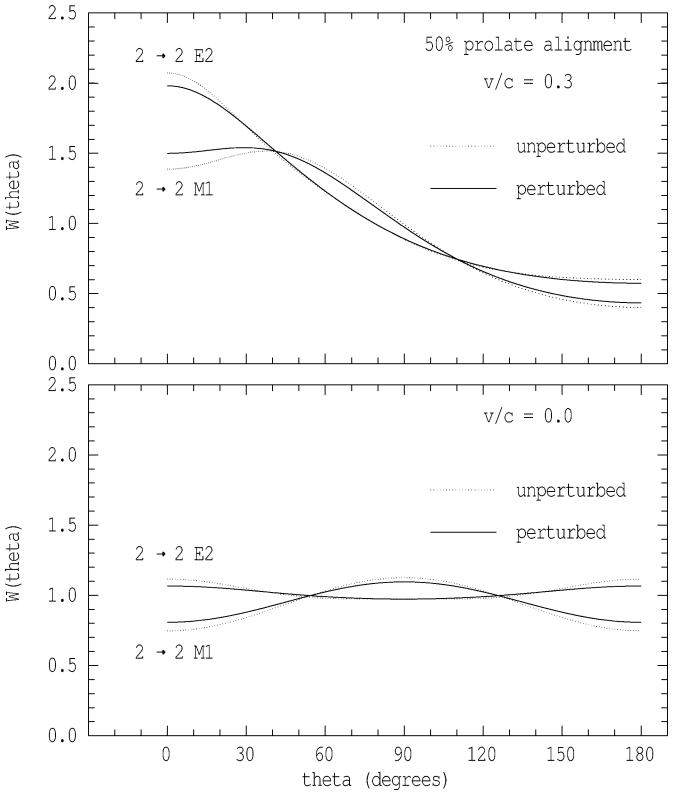

Fig. 14. Examples of angular distributions perturbed by free-ion (recoil in vacuum) fields. The perturbation is the maximum possible for a hydrogen-like electron configuration. The distributions in the rest frame of the nucleus are shown in the lower panel and the laboratory-frame distributions for ions moving at 30% of the speed of light are shown in the upper panel.

the ion carries many electrons in a complex excited configuration which de-excites on the time-scale of picoseconds [36].

For both hot and cold ionization, the perturbed angular distribution can be written in the form (cf. Eq. (20))

$$W(\theta) = \sum_k B_k(I_i) A_k(\delta_\gamma L L' I_f I_i) Q_k(E_\gamma) G_k(\omega\tau) P_k(\cos\theta), \tag{43}$$

where the perturbation is specified by an integral deorientation coefficient $G_k(\omega\tau)$. For the case of cold ionization

$$G_k(\omega\tau) = 1 - \frac{k(k+1)}{(2I_i+1)^2} \frac{(\omega\tau)^2}{1+(\omega\tau)^2}, \tag{44}$$

where τ is the mean life of the nuclear state I_i and the Lamor frequency is

$$\omega = -g \frac{\mu_N}{\hbar} (2I_i + 1) B_{hf}. \tag{45}$$

$B_{\rm hf}$ is the hyperfine field at the nucleus. As $\omega\tau \to \infty$, G_k reaches a hard core value of

$$G_k(\infty) = 1 - \frac{k(k+1)}{(2I_i+1)^2}. \tag{46}$$

Thus for $I = 2$, $G_2(\infty) = 0.76$ and $G_4(\infty) = 0.2$, while for $I = 2.5$, $G_2(\infty) = 0.833$ and $G_4(\infty) = 0.444$. The integral perturbations due to the cold ionization process are therefore modest, as indicated in Fig. 14. The fact that the $k = 4$ term in the angular distribution is already small when the alignment is $\lesssim 50\%$ also helps make the effect of the recoil in vacuum perturbation small.

The attenuation coefficients in the hot ionization regime are often described by the Abragam and Pound theory [37], which gives integral attenuation coefficients of

$$G_k = \frac{\lambda}{\lambda + \eta_k} = \frac{\tau_k}{\tau_k + \tau}, \tag{47}$$

where $\lambda = 1/\tau$ is the decay rate of the nuclear state and $\eta_k = 1/\tau_k$ are the vacuum deorientation decay rates given by

$$\eta_k = \frac{1}{3}k(k+1)\tau_c\omega_m^2, \tag{48}$$

where

$$\omega_m = \frac{g\mu_{\rm N}\langle H^2\rangle^{1/2}}{\hbar} \tag{49}$$

is the Lamor frequency, which depends on the root mean square of the hyperfine magnetic field at the nucleus, $\langle H^2\rangle^{1/2}$, and τ_c, the mean time between the random fluctuations of the hyperfine magnetic field.

In contrast with cold ionization, the hot ionization process has the potential to reduce the nuclear alignment more significantly because for $\tau \gg \tau_k$, $G_k \to 0$. It is also possible that sufficiently slowly moving ions can be sustained in a hot ionization regime by frequent collisions with residual gas in a relatively poor vacuum. The very small alignments ($\sim 2\%$) observed in the TDPAD measurements of Ref. [32] have been attributed to this mechanism.

6. Summary and conclusion

This paper has set out the formalism for γ-ray angular correlations and angular distributions with a view to applications to exotic nuclei produced as fast fragments [10, 14,15]. Several examples of angular distributions and correlations have been presented and discussed.

Provided a significant spin alignment can be achieved as a result of the reaction mechanism, and there are strong indications that this can be achieved [4,7,9], then γ-ray multipolarities and level spin assignments based on angular correlations/distributions will be feasible. One complication, compared with conventional low-energy fusion–evaporation, is that the alignment cannot always be assumed to be oblate and relatively large. It is evidently affected by the mechanism of the fragmentation process and by the momentum range selected by the fragment separator.

Arguably, the most important issue for future applications of γ-ray angular correlations/distributions to spectroscopy studies on excited fragments is to reach a quantitative understanding of the spin alignment and polarization mechanisms. Some theoretical aspects of this are discussed in Ref. [15] and experimental studies are underway [10]. Applications to intermediate-energy Coulomb excitation are considered in Ref. [38].

Acknowledgements

This work was motivated by discussions with many colleagues, especially Paul Mantica, Daniel Groh, Heather Olliver, Thomas Glasmacher, Robert Janssens and Gregers Hansen. It was supported in part by the US National Science Foundation Grants Nos. PHY01-10253 and PHY99-83810.

References

[1] K. Asahi, M. Ishihara, N. Inabe, T. Ichihara, T. Kubo, M. Adachi, H. Takanashi, M. Kouguchi, M. Fukuda, D. Mikolas, D.J. Morrissey, D. Beaumel, T. Shimoda, H. Miyatake, N. Takahashi, Phys. Lett. B 251 (1990) 488.
[2] K. Asahi, M. Ishihara, T. Ichihara, M. Fukuda, T. Kubo, Y. Gono, A.C. Mueller, R. Anne, D. Bazin, D. Guillemaud-Mueller, R. Bimbot, W.D. Schmidt-Ott, J. Kasagi, Phys. Rev. C 43 (1991) 456.
[3] H. Okuno, K. Asahi, H. Sato, H. Ueno, J. Kura, M. Adachi, T. Nakamura, T. Kubo, N. Inabe, A. Yoshida, T. Ichihara, Y. Kobayashi, Y. Ohkubo, M. Iwamoto, F. Ambe, T. Shimoda, H. Miyatake, N. Takahashi, J. Nakamura, D. Beaumel, D.J. Morrissey, W.D. Schmidt-Ott, M. Ishihara, Phys. Lett. B 335 (1994) 29.
[4] W.-D. Schmidt-Ott, K. Asahi, Y. Fujita, H. Geissel, K.-D. Gross, T. Hild, H. Irnich, M. Ishihara, K. Krumbholz, V. Kunze, A. Magel, F. Meissner, K. Muto, F. Nickel, H. Okuno, M. Pfützner, C. Scheidenberger, K. Suzuki, M. Weber, C. Wennemann, Z. Phys. A 350 (1994) 215.
[5] K. Asahi, H. Ueno, H. Izumi, H. Okuno, K. Nagata, H. Ogawa, Y. Hori, H. Sato, K. Mochinaga, M. Adachi, A. Yoshida, G. Liu, N. Aoi, T. Kubo, M. Ishihara, W.D. Schmidt-Ott, T. Shimoda, H. Miyatake, S. Mitsuoka, N. Takahashi, Nucl. Phys. A 588 (1995) 135c.
[6] G. Neyens, N. Coulier, S. Ternier, K. Vyvey, S. Michiels, R. Coussement, D.L. Balabanski, J.M. Casandjian, M. Chartier, D. Cortina-Gil, M. Lewitowicz, W. Mittig, A.N. Ostrowski, P. Roussel-Chomaz, N. Alamanos, A. Lépine-Szily, Phys. Lett. B 393 (1997) 36.
[7] F. Azaiez, in: Zs. Dombradi, A. Krasznahorkay (Eds.), Proceedings of the International Symposium on Exotic Nuclear Structures, Debrecen, Hungary, 2000, MTA Atomki, Debrecen, 2000, p. 149;
F. Azaiez, Nucl. Phys. A 704 (2002) 37c;
F. Azaiez, et al., Eur. Phys. J. A 15 (2002) 93.
[8] M. Belleguic, M.-J. Lòpez-Jiménez, M. Stanoiu, F. Azaiez, M.-G. Saint-Laurent, O. Sorlin, N.L. Achouri, J.-C. Angélique, C. Bourgeois, C. Borcea, J.-M. Daugas, C. Donzaud, F. De Oliveira-Santos, J. Duprat, S. Grévy, D. Guillemaud-Mueller, S. Leenhardt, M. Lewitowicz, Yu.-E. Penionzhkevich, Yu. Sobolev, Nucl. Phys. A 682 (2001) 136c.
[9] D. Sohler, et al., Phys. Rev. C 66 (2002) 054302.
[10] H. Olliver, T. Glasmacher, A.E. Stuchbery, in: A. Aprahamian, J.A. Cizewski, S. Pittel, N.V. Zamfir (Eds.), Mapping the Triangle: International Conference on Nuclear Structure, in: AIP Conference Proceedings, Vol. 638, 2002, p. 249;
H. Olliver, T. Glasmacher, A.E. Stuchbery, Bull. Am. Phys. Soc. 47 (6) (2002) 100.
[11] P.G. Hansen, B.M. Sherrill, Nucl. Phys. A 693 (2001) 133, and references therein.
[12] V. Maddalena, et al., Phys. Rev. C 63 (2001) 024613.
[13] M. de Jong, A.V. Ignatyuk, K.-H. Schmidt, Nucl. Phys. A 613 (1997) 435.
[14] D.E. Groh, P.F. Mantica, A.E. Stuchbery, et al., in preparation.

[15] A.E. Stuchbery, D.E. Groh, P.F. Mantica, in preparation.
[16] G.A. Souliotis, D.J. Morrissey, N.A. Orr, B.M. Sherrill, J.A. Winger, Phys. Rev. C 46 (1992) 1382.
[17] M. Lewitowicz, et al., Nucl. Phys. A 682 (2001) 175c, and references therein.
[18] M. Pfützner, et al., Phys. Rev. C 65 (2002) 064604, and references therein.
[19] A.E. Stuchbery, M.P. Robinson, Nucl. Instrum. Methods A 485 (2002) 753.
[20] K. Alder, A. Winther, Electromagnetic Excitation, North-Holland, Amsterdam, 1975.
[21] W.D. Hamiltion (Ed.), The Electromagnetic Interaction in Nuclear Spectroscopy, North-Holland, Amsterdam, 1975.
[22] K.S. Krane, R.M. Steffen, R.M. Wheeler, Nucl. Data Tables 11 (1973) 351.
[23] T. Yamazaki, Nucl. Data A 3 (1967) 1.
[24] G. Neyens, R. Nouwen, R. Coussement, Nucl. Instrum. Methods Phys. Res. A 340 (1994) 555.
[25] M.J.L. Yates, in: K. Siegbahn (Ed.), Alpha-, Beta-, and Gamma-Ray Spectroscopy, Vol. 2, North-Holland, Amsterdam, 1965, p. 1691.
[26] H. Morinaga, T. Yamazaki, In-Beam Gamma-Ray Spectroscopy, North-Holland, Amsterdam, 1976.
[27] D. Pelte, D. Schwalm, in: R. Bock (Ed.), Heavy Ion Collisions, Vol. 3, North-Holland, Amsterdam, 1982, p. 1.
[28] Y. Niv, M. Hass, A. Zemel, G. Goldring, Phys. Rev. Lett. 43 (1979) 326.
[29] E. Dafni, G. Goldring, M. Hass, O.C. Kistner, Y. Niv, A. Zemel, Phys. Rev. C 25 (1982) 1525.
[30] H. Scheit, T. Glasmacher, B.A. Brown, J.A. Brown, P.D. Cottle, P.G. Hansen, R. Harkewicz, M. Hellström, R.W. Ibbotson, J.K. Jewell, K.W. Kemper, D.J. Morrissey, M. Steiner, P. Thirolf, M. Thoennessen, Phys. Rev. Lett. 77 (1996) 3967;
H. Scheit, PhD thesis, Michigan State University, 1998, unpublished.
[31] T. Motobayashi, Eur. Phys. J. A 15 (2002) 99.
[32] G. Neyens, et al., Nucl. Phys. A 701 (2002) 403c.
[33] P.G. Hansen, Phys. Rev. Lett. 77 (1996) 1016.
[34] D. Bazin, W. Benenson, B.A. Brown, J. Brown, B. Davids, M. Fauerbach, P.G. Hansen, P. Mantica, D.J. Morrissey, C.F. Powell, B.M. Sherrill, M. Steiner, Phys. Rev. C 57 (1998) 2156.
[35] P.G. Hansen, private communication.
[36] G. Goldring, in: R. Bock (Ed.), Heavy Ion Collisions, Vol. 3, North-Holland, Amsterdam, 1982, p. 483.
[37] A. Abragam, R.V. Pound, Phys. Rev. 92 (1953) 943.
[38] H. Olliver, T. Glasmacher, P.G. Hansen, A.E. Stuchbery, in preparation.